

This is the peer reviewed version of the following article:

Impedance Investigation of MIFM Ferroelectric Tunnel Junction using a Comprehensive Small-Signal Model / Benatti, L.; Puglisi, F. M.. - In: IEEE TRANSACTIONS ON DEVICE AND MATERIALS RELIABILITY. - ISSN 1530-4388. - 22:3(2022), pp. 332-339. [10.1109/TDMR.2022.3182941]

Terms of use:

The terms and conditions for the reuse of this version of the manuscript are specified in the publishing policy. For all terms of use and more information see the publisher's website.

27/04/2026 04:28

(Article begins on next page)

Impedance Investigation of MIFM Ferroelectric Tunnel Junction using a Comprehensive Small-Signal Model

Lorenzo Benatti, Francesco Maria Puglisi

Dipartimento di Ingegneria “Enzo Ferrari”, Via P. Vivarelli 10/1, 41125 – Modena (MO) - Italy

Corresponding author email: lorenzo.benatti@unimore.it phone: +39-059-2056324

Abstract— The urge to develop efficient and ultra-low power architectures for modern and future technological needs lead to an increasing interest and investigation of neuromorphic and ultra-low power computing. In this respect, ferroelectric technology is found to be a perfect candidate to guide this technological transition. Elucidating the physical mechanisms occurring during ferroelectric-based devices operations is fundamental in order to improve the reliability of emerging architectures. In this work, we investigate metal/insulator/ferroelectric/metal (MIFM) ferroelectric tunnel junctions (FTJs) consisting of a ferroelectric hafnium zirconium oxide (HZO) layer and an alumina (Al_2O_3) layer by means of C-f and G-f measurements performed at multiple voltages and temperatures. For a trustworthy interpretation of the measurements results, an innovative small signal model is introduced that goes beyond the state of the art by *i*) separating the role played by the leakage in the two layers; *ii*) including the impact of the series impedance (that depends on the samples layout); *iii*) including the frequency dependence of the dielectric permittivity; *iv*) accounting for the fact that not the whole HZO volume crystallizes in the orthorhombic ferroelectric phase. The model correctly reproduces measurements taken on different devices in different conditions. Results highlight that the typical estimation method for interface trap density may be misleading.

Keywords – Ferroelectric Tunnel Junction, Capacitance, Small signal model, Neuromorphic.

I. INTRODUCTION

Modern technological needs have recently pushed the research toward the exploration of innovative and energy-efficient computational architectures, mainly focusing on the development of circuits for artificial intelligence applications running on edge devices. In this respect, this paradigm transition can be aimed at by leveraging on the adaptive learning of ferroelectric materials polarization, that allows non-volatile multilevel memory effect [1] and opens to the possibility of bypassing the device and circuit-level limitations of CMOS technology, such as difficulties in further scaling (at the device level) and the intrinsic physical separation of computation and memory units that prevents an energy efficient data manipulation (the so called von Neumann bottleneck). In particular, the latter has been identified as the most important limit of conventional CMOS architectures in terms of energy efficiency.

In this respect, the hafnium zirconium oxide (HZO)-based Ferroelectric Tunnel Junction (FTJ) memories with Metal/Insulator/Ferroelectric/Metal (MIFM) structure are found to be promising candidates to act as ultra-low power synaptic elements in analog neuromorphic architectures [2], such as devices for Logic in Memory (LiM) operations and as stand-alone memories. With respect to a MFM structure, the presence of an additional insulator (dielectric) layer, required to induce a polarization dependence of the electrical resistance of the device allowing non-destructive readout [3,4], further complicates the analysis of the physical mechanisms occurring in these devices and reduces, as a downside, their reliability. In fact, achieving reliable and functional circuits requires a satisfactorily large compensation of the polarization charges, that is indeed instrumental to the device retention. The latter is however hindered by the presence of the dielectric layer and therefore intrinsically related to the dynamics of charge trapping in the defects that are present in the different layers and at the insulator/ferroelectric (IF) interface. However, the full understanding of their role and of the underlying mechanisms, critical for reliable device operation, is far from being achieved.

Elucidating, then, the physical mechanisms occurring during device operation is of fundamental importance to improve the reliability of ferroelectric devices and for their actual introduction in advanced and dependable neuromorphic and ultra-low power circuits.

In this work, we investigate the role of traps and material properties by studying the small signal response of FTJs consisting of an HZO ferroelectric (FE) and alumina (Al_2O_3) dielectric (DE) bi-layer structure by means of C-f and G-f measurements performed at multiple voltages and temperatures. Experiments are carried out extending the typical 1 MHz limit up to 10 MHz, allowing a deeper and more detailed investigation of the frequency response of these devices. High frequency measurements are found to be fundamental to properly verify the impact of material properties and related parameters on the device behaviour. Indeed, some features may become evident only at high enough frequencies that are usually not investigated. High frequency studies can be also useful for Deep Neural Networks (since they typically operate at much larger frequencies than Spiking Neural Networks) as well as for LiM and non-volatile memory applications. For a dependable interpretation of the results, a novel small signal model has

*Copyright © 2022 IEEE. Personal use of this material is permitted. However, permission to use this material for any other purposes must be obtained by sending a request to pubs-permissions@ieee.org

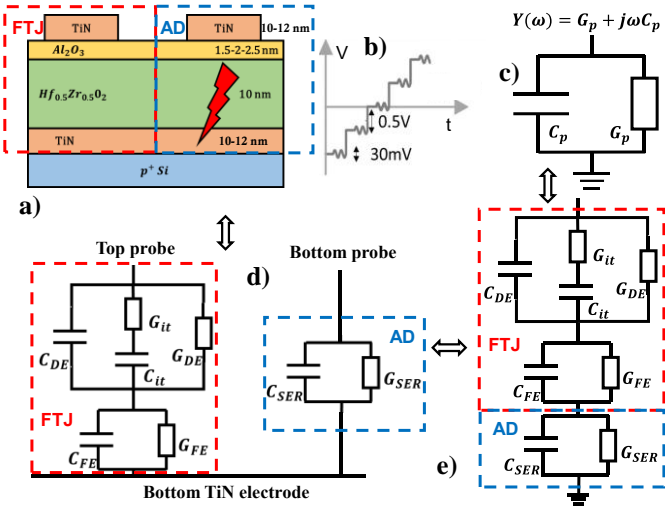


Fig. 1 - a) Sectional schematic of the FTJ stack. The access to the bottom electrode is achieved by breaking an access device (AD). b) Schematic representation of the waveform used in C-f and G-f measurements carried out on samples with different area and dielectric thickness. The applied DC voltage goes from -4V to 4V for $t_{DE} = 1.5 \text{ nm}$, -4.5V to 4.5V for other thicknesses, with 0.5V steps. An AC signal of 30 mV (RMS) with frequency spanning from 1kHz to 10MHz is superimposed at each bias. It is then possible to obtain the frequency dependence of the total stack under measurement, considered as a general complex impedance, and so as the parallel of an equivalent C_p and G_p , (c) of the entire DUT. d) Equivalent small-signal circuit of the measured sample. The actual FTJ is connected to the top probe while the AD to the bottom probe (ground). The AD is considered as a complex impedance in series with the device under investigation. The C_{it} - G_{it} branch allows to model the equivalent trapped/interfacial charges and their τ . e) Corresponding small signal model proposed in this work.

been developed and validated, that includes several novelties as compared to the state of the art by *i*) introducing the separation of the role of the leakage in the two layers (DE and FE); *ii*) including the significant impact of the series impedance in the device under test (DUT) (that depends on the samples layout); *iii*) including the frequency dependence of the dielectric permittivity; *iv*) considering the well-known fact that not the whole HZO volume crystallizes in the orthorhombic ferroelectric phase. The model is shown to correctly reproduce measurements taken on different devices in different conditions.

The paper extends our previous conference paper [5] by providing a more detailed explanation on the model parameter's extraction methodology, together with the sensitivity analysis that encompasses all the parameters in the model and other modeling attempts comparison.

The paper is then organized as follows: in Section II, we introduce the devices and the performed experiments that lead to the development of the proposed new small-signal model, which is then described in Section III; its implementation and validation is shown in Section IV, while in Section V a detailed sensitivity analysis of each model parameter is reported, and its discussion is used to elucidate the role of the different layers in the measured response. In Section VI we report the results obtained by measuring and modeling different devices across the wafer, together with the results and discussions of the temperature-dependent measurements. Conclusions follow.

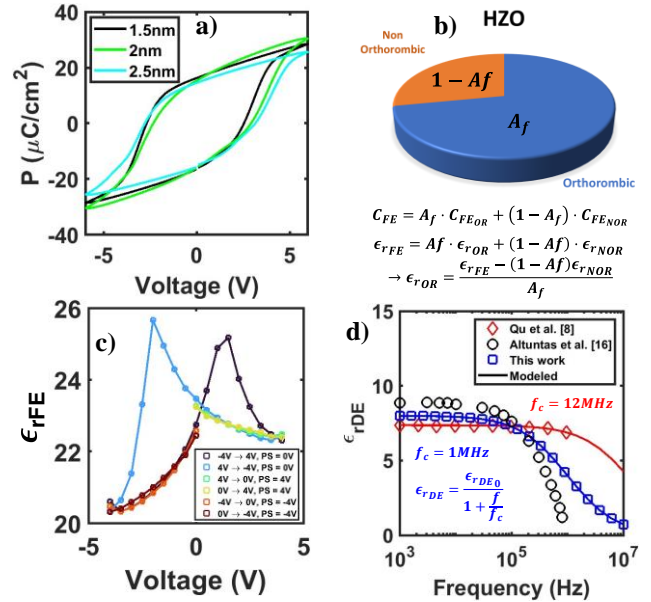


Fig. 2 - a) Polarization-voltage curves measured after wake-up on samples with different DE thickness, showing a satisfying ferroelectric switching. b) The crystallization phase of the HZO is known to be not uniform, thus the ferroelectric HZO is considered not completely orthorhombic. An area factor ($A_f=50\text{--}90\%$ [11,12]) is then introduced to consider the contribution of this non-ideality. Reported equations show how the corresponding effective permittivity (ϵ_{rFE}) can be calculated. c) C-f G-f measurements have been carried out with different starting and pre-poling voltages. The extracted ϵ_{rFE} voltage dependence matches expectation and is consistent with literature results [11,14]. The extracted values are lower than those reported for purely orthorhombic HZO due to A_f . d) The DE permittivity is considered frequency dependent [8,16] using a single pole model in order to include the effect of the ALD. Although this is not an universal $\epsilon_{rDE}(f)$ model, the extracted corner frequencies allow to derive profiles in the range of values already presented in the literature [8,16].

II. DEVICE AND EXPERIMENTS

The FTJs analyzed in this work, fabricated and provided by NaMLab, consist in a TiN/ Al_2O_3 /10nm-HZO/TiN stack presenting 3 different Al_2O_3 thicknesses (1.5-2-2.5nm). The cross-sectional schematic is shown in Fig. 1a. The TiN (10-12nm) bottom electrode (BE) was sputtered at room temperature using physical vapor deposition (PVD), while the HZO (FE) and the Al_2O_3 (DE) layers were deposited by atomic layer deposition (ALD) on p^+ -Si wafers. Then, the top TiN electrodes (TEs, 10-12nm) were sputtered on top using the same process conditions as for the BE. After deposition, all samples were annealed to crystallize the HZO film. More details on the entire process are presented in [6]. In order to contact the BE, common to all the devices but not directly accessible, hard breakdown must be induced in a sacrificial device (henceforth, access device – AD), as shown in Fig. 1a. In order to have a satisfying repeatability in the C-f and G-f measurements and to investigate the devices in a state in which they are considered to be fully functional [6,7], all devices are woken up with a train of 3000 triangular pulses ($\pm 6\text{V}$, 10kHz). After wake-up, the FTJs exhibit good ferroelectric switching and a large remnant polarization $2P_r \approx 35 \mu\text{C}/\text{cm}^2$ as shown in Fig. 2a.

Then, to study the small-signal behavior of the entire DUT and the material properties, C-f/G-f measurements (Fig. 1b) are carried out at different DC voltages (-4.5 V to 4.5 V for $t_{DE}=2\text{--}2.5\text{nm}$ and -4V to 4V for $t_{DE}=1.5\text{nm}$), temperatures (30°C to 100°C), and frequencies up to 10 MHz, introducing an important novelty since in existing works the typical limit

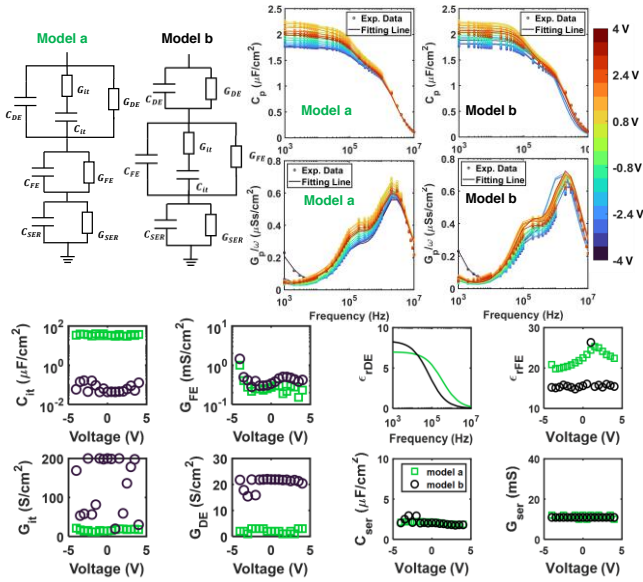


Fig. 3 –Small-signal model adopted in this study (model a) and a different attempt (model b), in which the C_{it} - G_{it} branch was shifted from the DE to the FE side. On the right, comparison of modelling results at different voltages on the same measured dataset are reported, together with extracted parameters. Green squares (black circles) refer to model a (model b).

is 1 MHz [8,9]. The admittance of the entire stack is measured as the parallel of a capacitance (C_p) and a conductance (G_p), as shown in Fig. 1c, and includes the contribution of the AD and other possible layout parasitic not compensated for by short-circuit and open-circuit compensation, that are however performed before the measurements.

III. PROPOSED SMALL-SIGNAL MODEL OF THE FTJ

To interpret the results and to study the role of each layer, we introduce a small-signal model (see Fig. 1d-e) with significant novelties with respect to those already present in the literature [8,9]. Specifically, *i*) to fully consider the effect of the AD and, in general, of possible stray and interconnect impedance that is always present even in layouts in which the BE is directly accessible, we include a general complex impedance, modelled as the parallel of C_{SER} and G_{SER} , in series with the actual FTJ stack; *ii*) each FTJ layer is modeled by considering their capacitance and parallel conductance, the latter being representative of the leakage through that specific layer. This introduces a significant novelty as compared to other reports in the literature [8,9] in which the leakage was included by considering a single and global parallel conductance tied across the whole stack, making impossible to investigate the role played by each layer in charge transport; *iii*) we take into account the well-known fact [10] that HZO does not crystallize fully in the orthorhombic (and ferroelectric) phase, but also exhibits non-orthorhombic monoclinic and tetragonal grains with different permittivity values [11]. So, we determine the FE relative permittivity (ϵ_{rFE}) as shown in Fig. 2b, where ϵ_{rOR} and ϵ_{rNOR} are the permittivity of the orthorhombic (i.e., usually around 36 [12]) and non-orthorhombic phases, respectively, and A_f (area factor) is defined as the fraction of the area occupied by orthorhombic grains. This parameter can be then estimated by fitting the model parameters to experimental data [13]. These values are considered for simplicity to be frequency-

independent, as it was shown up to a few GHz using dedicated test structures [14]. In addition, ϵ_{rFE} is considered voltage dependent [12,15]. Fig. 2c shows how the optimization algorithm (see Section IV) used to extract our model parameters reproduces the expected ϵ_{rFE} voltage dependent profiles reported in the literature [12,15] without any a priori constraint, which further strengthens the validity of the proposed approach. C-f/G-f measurements using different pre-poling and DC voltage range combinations have been performed to test the reliability and repeatability of the model. The perfect overlap of the values extracted at the same voltage in all measurements underlines that the values are self-consistent and validates the overall modeling method. This also confirms that applying a specific DC bias at each step of the C-f/G-f measurement (Fig. 1b) is sufficient to determine the number of switched ferroelectric domains even before the application of the superposed AC signal, which makes the measured frequency response free from artifacts that may come from stray polarization; *iv*) we include the frequency dependence of the DE permittivity, which depends on the DE thickness and deposition process, by using a single-pole model, see Fig. 2d. ϵ_{rDE} is then derived as the combination of two parameters, ϵ_{rDE0} that is the value of ϵ_{rDE} at zero frequency, and the corner frequency, f_c . This allows to obtain profiles in agreement with data from the literature [8,16], that clearly show how the corner frequency (f_c) (or, more generally, the frequency roll-off) may easily be in the range explored in this work.

In agreement with other works [8,9], the role of the defects located both in the DE/FE layers and at the IF interface is included by means of a lumped C_{it} - G_{it} branch across the DE. Different attempts in positioning this branch have been done, but with unsatisfying results. Fig. 3 shows in fact that positioning the traps branch across the FE side results in a model that fails at reproducing the expected ϵ_{rFE} voltage dependence, although resulting in overall satisfying fitting of the C-f and G-f measurements. In addition to this result, which would be sufficient to discard this alternative formulation of the model, we noticed that with this approach the other extracted parameters are inconsistent with expectations. In particular, the corner frequency that models the frequency dependence of ϵ_{rDE} (f_c) is unrealistically low (about 30 kHz), so largely below the values reported in the literature (Fig. 2d). Furthermore, G_{it} voltage trend results too scattered and with notably high values. In addition, the extracted C_{it} value is suspiciously lower than $1\mu F/cm^2$ ($\sim 0.1\mu F/cm^2$), which would lead to an erroneous evaluation of the trapped charge density. Such a value would actually suggest a remarkably clean interface between Al_2O_3 and HZO that is very difficult to achieve given the different nature of the two materials and the large number of different atomic species in place. Moreover, C_{it} (and therefore D_{it}) should in fact be regarded as given by an effective trap density that somehow includes also the contribution of bulk traps in HZO layer (as if they were lumped at the interface) and is also responsible for the compensation of polarization charges (that are in the order of few tens of $\mu F/cm^2$). Very small D_{it} values would make the polarization charges largely uncompensated, preventing the correct device operation. To compare our results with those obtained using the approaches in references [8,9], alternative small-signal model formulations that employ a generalized

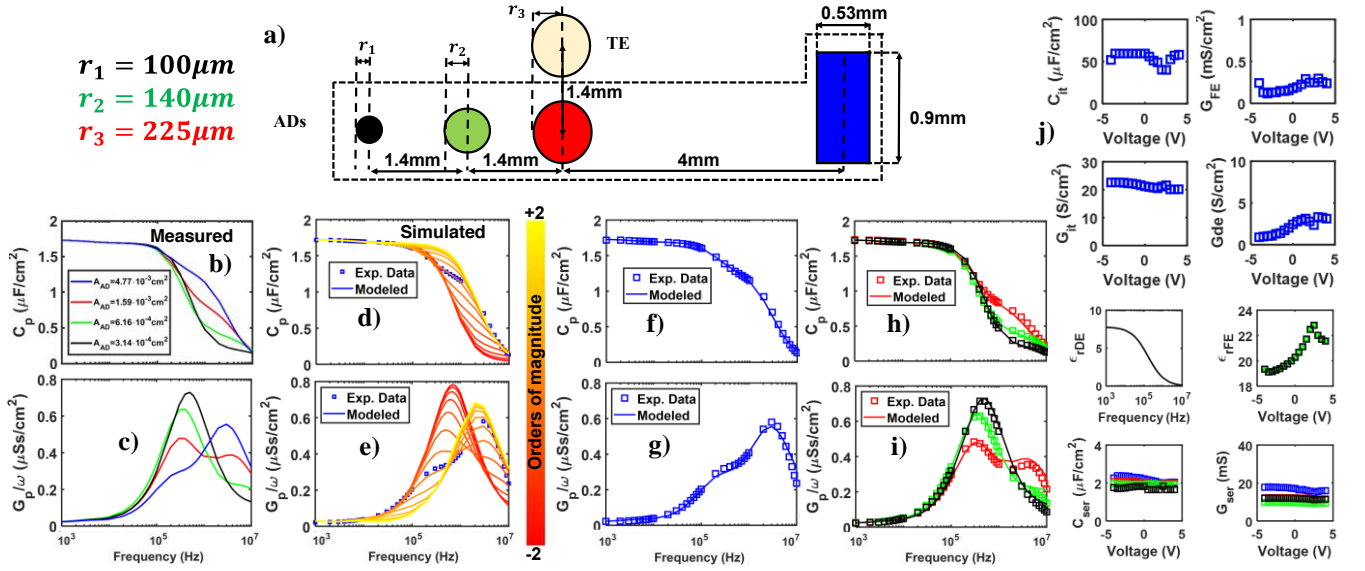


Fig. 4 - a) Top view of employed ADs used to measure the same device (TE). b-c) Experimental data obtained at -2V using ADs with different areas (different C_{SER} – the same color code as in (a) is used). d-e) Measured (blue symbols) and simulated (solid lines) C_p (d) and G_p/ω (e) profiles. Simulation allows to derive the measurement C_{SER} value, which is then varied over ± 2 orders of magnitude to investigate the impact of this parameter on C_p and G_p/ω profiles (red to yellow lines). All other parameters are left unchanged to the values extracted by the fitting. f-g-h-i) Modeling (lines) of data (symbols) obtained using ADs with different areas (same color code as in (a) is used). Initially, measured data (symbols) in (f) and (g) are fitted at different applied voltages (-4V to 4V), resulting in the parameters reported in (j) (blue symbols and line). Then, by only varying the series impedance parameters (bottom boxes in (j)) and leaving fixed all the others the C_p and G_p/ω profiles corresponding to ADs with different areas are well reproduced (h) and (i)). j) Extracted model parameters. As expected, C_{SER} decreases proportionally to the AD area, as the area-normalized C_{SER} is constant, and comparable to C_p at low frequencies. G_{SER} s are also comparable, since all ADs are broken with the same I_c .

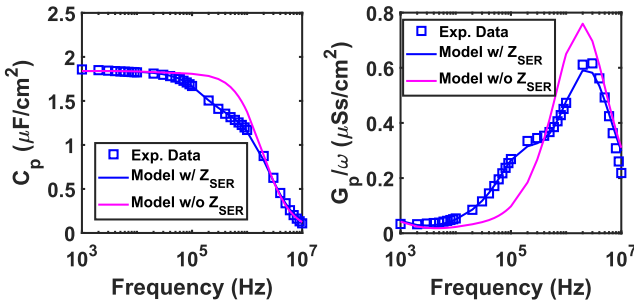


Fig. 5 Comparison of measured C_p and G_p/ω profiles (blue symbols) with modeling results (blue line) and the actual DUT response (magenta) without the contribution of the AD. Shown results are for the blue profiles in Fig. 4.

leakage conductance spanning across the whole FTJ stack (instead of using dedicated a leakage conductance for each layer) have been tried, without interesting outcomes.

IV. SMALL-SIGNAL MODEL VALIDATION

The model validation is conducted exploiting the possibility, given by the samples layout, to control the series impedance by choosing ADs with different areas (different C_{SER}) and break them with the same current compliance $I_c = 10$ mA (that, in first approximation, defines G_{SER}). To better evidence the impact of the AD area on the frequency response, the C_p and G_p/ω profiles measured at -2 V (i.e., the typical read voltage [17]) on an FTJ with $t_{DE}=1.5$ nm, using ADs with 4 different areas (sketch in Fig. 4a) are reported in Fig. 4b-c.

Notably, the response significantly changes with the area of the AD (and thus with C_{SER}), underlining the significant impact of the series impedance on the entire measurement. This is further confirmed by the sensitivity analysis carried out on C_{SER} , obtained by varying only the obtained value over ± 2 order of magnitude, which clearly shows how the variation of

this parameter alone has a profound impact on C_p and G_p/ω profiles. The obtained profiles (red to yellow lines) are clearly in agreement with the experimental results, Fig. 4d-e. To further confirm the impact of the AD area, C_{SER} values were extracted by a global minimization algorithm to reproduce the data at all voltages corresponding to the largest AD, (an example is shown by the blue line and symbols for an applied voltage of -2V in Fig. 4f-g). To obtain the model parameters, we used a least square non-linear minimization implemented in MATLAB using the function *lsqnonlin*(). For each voltage, both measured C_p and G_p/ω profiles are simultaneously given as input to the algorithm, where the admittance of our model is described as a function of the model parameters. Then the algorithm varies the nine parameters (indeed ϵ_{rDE} is modelled using two parameters, i.e., ϵ_{rDE0} that is the value of ϵ_{rDE} at zero frequency, and the corner frequency, f_c) in the model within previously determined boundaries (estimated as educated guesses on the expected values for the parameters) to obtain the minimum difference between the measured profiles and the curves obtained by using the model. This procedure is repeated separately for each DC voltage. All extracted parameters are reported in Fig. 4j. Remarkably, the model can reproduce the profiles measured at different AD areas by keeping all the parameters fixed and letting only the series impedance parameters (C_{SER} and G_{SER}) vary freely, Fig. 4h-i. Moreover, the extracted values of C_{SER} (per unit area) do not change with the AD area and are compatible with the value of the series of C_{DE} and C_{FE} (per unit area) at low frequencies. Also, all the extracted G_{SER} values are similar, as expected since the devices were all broken at the same I_c . These results validate the model ability to consider the contribution of the AD and, in general, of whatever series impedance may be present during the measurement. Furthermore, this modelling approach is fundamental since even a series impedance of few

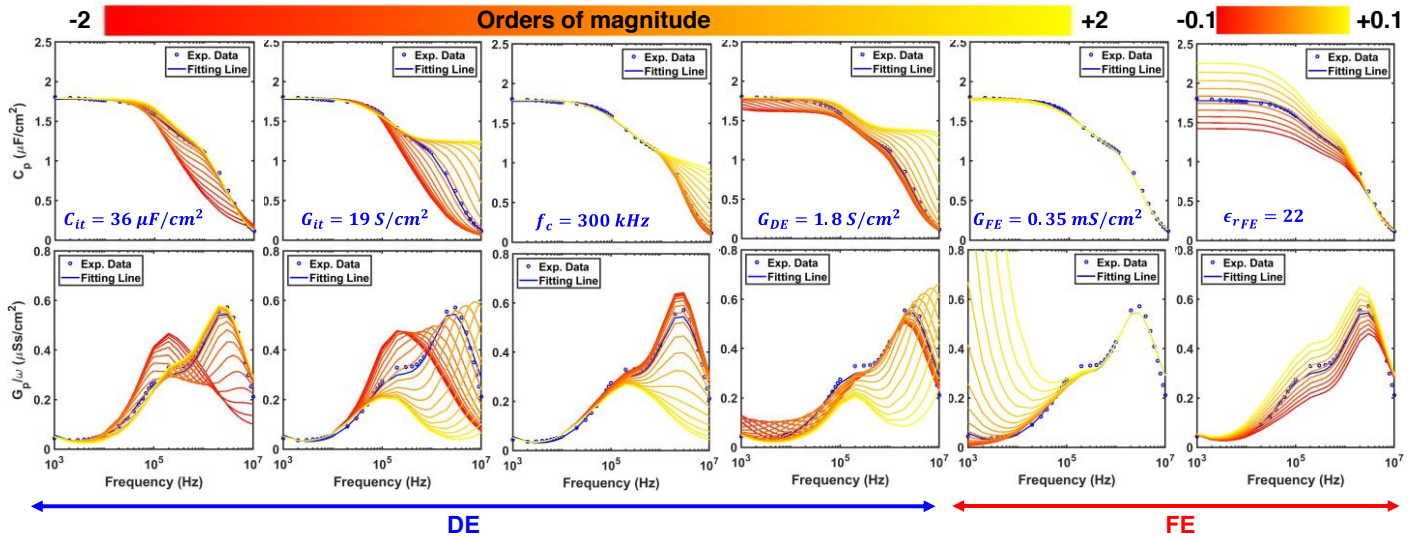


Fig. 6 – Sensitivity analysis on C_p and G_p/ω of model parameters over ± 2 orders of magnitude. Red to yellow lines are obtained modeling the experimental data of a device with $t_{DE} = 1.5nm$ and $A_{AD} = 4.77 \cdot 10^{-4}cm^2$ at $-4V$ (symbols), which leads to the starting profile (blue line), and then by changing only the parameter of interest. The parameters for the first modeled blue lines are reported in blue. DE parameters are evidenced by a blue arrow and FE parameters with a red arrow.

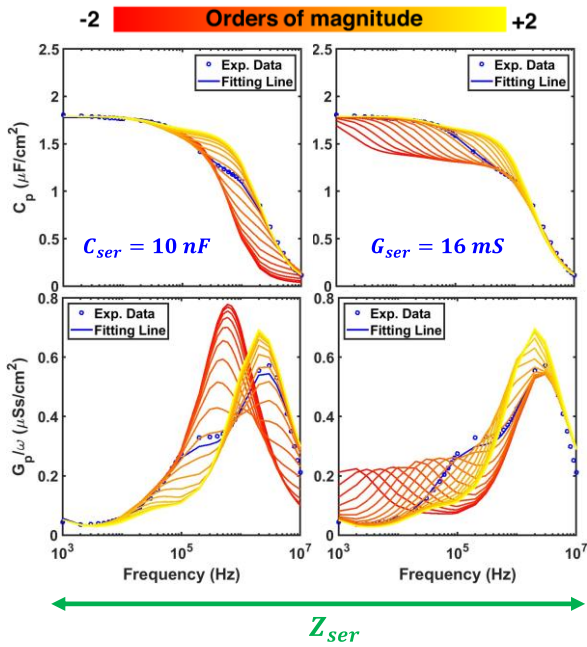


Fig. 7 – Sensitivity analysis on C_p and G_p/ω of series impedance model parameters over ± 2 orders of magnitude of a device with $t_{DE} = 1.5nm$ $A_{AD} = 4.77 \cdot 10^{-4}cm^2$ at $-4V$. Lines are obtained as previously explained in Fig. 6.

tens of pF is found to strongly impact the peak magnitude in the G_p/ω profile, typically used to estimate the interface trap density [8,9]. Also, depending on the series impedance value (in particular C_{SER}), a second peak may appear above 1 MHz, which would go unnoticed without extending the measurement range to 10MHz. In addition, as shown in Fig. 2c and 4j, the model qualitatively reproduces the expected ϵ_{rFE} voltage dependence [14], but with lower overall values as the HZO is not fully orthorhombic. Moreover, the extracted ϵ_{rDE} frequency profile is compatible with literature reports [8,16]. The flexibility of the proposed model also allows to analyze the intrinsic response of the actual FTJ eliminating the contribution of the AD. Fig. 5 shows the measured profiles (blue symbols) together with the model fitting (blue lines) and

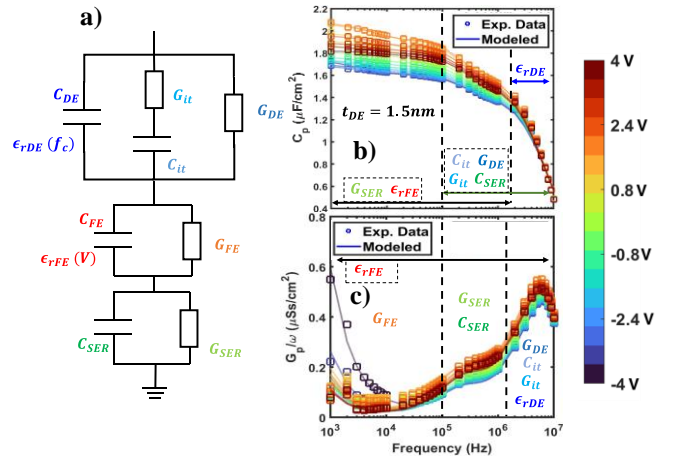


Fig. 8 – a) Employed small-signal model where each parameter is appropriately color coded. b-c) C-f/G-f results at different DC voltages for a device with $t_{DE} = 1.5nm$. Parameters names are placed in the regions where they show the most relevant impact.

the intrinsic device response (magenta lines) of a device with $t_{DE}=1.5nm$, measured using the largest AD and taken at $-2V$ (same blue profiles of Fig. 4). Magenta lines are obtained using the same parameters (blue symbols in Fig. 4j) obtained by modelling the experimental data (blue symbols), by just removing the AD (Z_{SER}) from the model. The presence of a single roll-off in C_p and a single G_p/ω peak, consistent with other reports [8,9] where the presence of an additional AD is not mentioned, strengthen the validity of our proposed methodology.

V. SENSITIVITY ANALYSIS

The possibility to isolate the impact of each model parameter on the frequency response is now exploited to gain insights on the role played by the different layers and by the traps performing a sensitivity analysis across ± 2 orders of magnitude. Results in Fig. 6-7 are obtained fitting the C_p and G_p/ω profiles at $-4V$ of a representative device with $t_{DE}=1.5nm$, and then varying a single parameter per time starting from the nominal extracted value. Outcomes are reported separating the effect of DE parameters (also

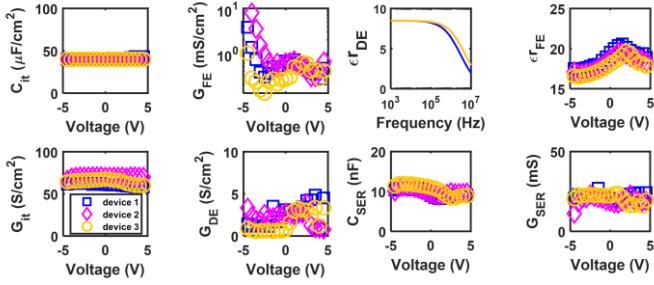


Fig. 9 – Comparison of voltage and frequency dependence of the model parameters extracted from measurements of different but nominally equal devices. All shown devices have $t_{DE} = 2.5 \text{ nm}$, $A = 6.16 \cdot 10^{-4} \text{ cm}^2$. The extracted parameters exhibit very small variability. Differences in G_{FE} at strongly negative bias can be attributed to different low frequency leakages, due to different devices states (the devices underwent different levels of fatigue during experiments).

considering the traps effects) and FE parameters. Results suggest, as expected, that the $C_{it} - G_{it}$ branch has a profound impact both on the position and on the number of peaks in the G_p/ω profile, and on the second C_p roll-off as well, the correct identification of which requires measurement frequencies beyond the typical 1 MHz limit. In particular, a negligible C_{it} would lead to a profile much more similar to the usually reported profiles [8,9] (although in this case the presence of the peak in the G_p/ω profile would be likely due to the series impedance effect alone), preliminarily suggesting a marked presence of defects in these devices. However, the study on DE properties highlights also the importance of G_{DE} and the frequency dependence of ϵ_{rDE} , especially at high frequencies, revealing a mixed and non-trivial effect of the dielectric properties and of the traps on the overall shape of both C_p and G_p/ω profiles. In fact, it is evident that the presence and the height (but not the position in frequency) of the second G_p/ω peak are strongly dependent on the cut off frequency of ϵ_{rDE} . This is a peculiar and noteworthy result, since the dielectric layer permittivity is usually considered to be frequency independent, at least in the frequency range adopted in these kinds of experiments and, all in all, in the frequency operating range expected for these devices [18]. Specifically, this result clarifies the importance of a careful process in which the dielectric properties may be controlled to guarantee the highest possible corner frequency value for the permittivity of the dielectric. Furthermore, the sensitivity analysis confirms that a frequency independent ($f_c \rightarrow \infty$) DE layer would lead to the presence of a single peak, completely suppressing the non-trivial effects given by the series impedance on the signature related to the traps (peak in the G_p/ω profile), also removing the second C_p roll off at high frequencies. The complex effect of the series impedance on the C_p and G_p/ω profiles is highlighted in Fig. 7, which shows how non-negligible series capacitance and limited series conductance values strongly impact the overall response, giving rise to unexpected behaviors that may lead to wrong estimations of the dielectric, ferroelectric, and traps parameters if not correctly accounted for. The FE parameters analysis in Fig. 6 reveals that the overall leakage is mostly sensitive to G_{FE} , dominated so by the defects in the FE layer rather than to G_{DE} . This is an expected result, since the HZO thickness is at least 4 times larger than the respective Al_2O_3 . HZO acts then as a bottleneck for leakage, and its conductance variations (hence the variation of

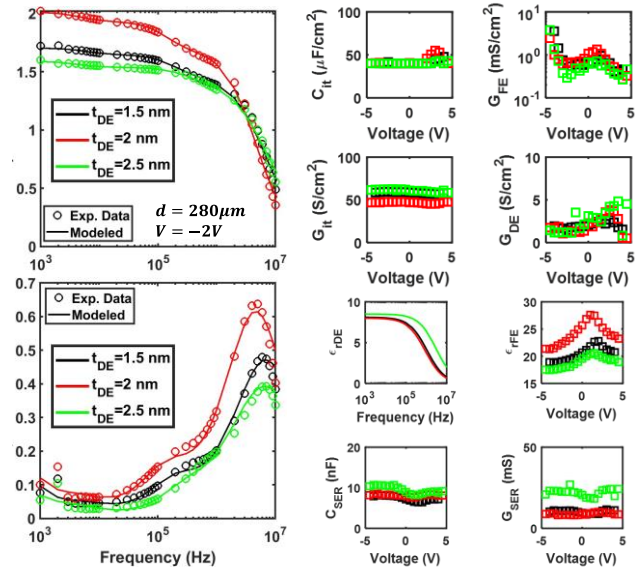


Fig. 10 – Example of C_p and G_p/ω profiles measured (symbols) and simulated (lines) at a DC voltage $V = -2V$ on devices with the same area and with different t_{DE} (different colors). On the right, model parameters extracted at different voltages are reported. No trend with the dielectric thickness is visible.

defect density within the layer) dictates the overall leakage through the stack.

This result also sheds light on the possible charge transport behavior, frequently discussed in the literature but still not completely understood [19] since in both polarization settings (positive and negative) the transport appears to be limited by the leakage in the FE layer, suggesting a decisive role of the trap-assisted tunneling processes in the FE for both positive and negative ferroelectric polarizations. The FE processing conditions and the resulting FE defectiveness have then a strong impact on the performance of the device. In addition, the impact of the ferroelectric permittivity is elucidated. Varying ϵ_{rFE} over a reduced range - because of its limited possible values - produces a vertical shift of both profiles. In particular, a value reduction (increase) causes a downward (upward) shift. This behavior is consistent with the resulting voltage dependance of ϵ_{rFE} , allowing the correct modeling of the profiles at different biases.

Fig. 8 shows an example of C-f/G-f measurements performed at biases from -4V to 4V and summarizes the regions of the C_p (Fig. 8b) and G_p/ω (Fig. 8c) profiles in which each model parameter, schematically reported in Fig. 8a, has a more significant influence than the others. It is worthwhile noticing that in both profiles the low frequency behavior is mostly dominated by the HZO properties, while the high frequency response derives from a non-trivial combination of the DE leakage, the frequency dependence of the DE permittivity, the trapped charge, and the series impedance contribution.

VI. RESULTS AND DISCUSSION

Measurements are repeated on different samples to validate the model stability and estimate device-level variability. As shown in Fig. 9, nominally equal FTJs exhibit very small parameters dispersion in general. However, G_{FE} s comparison reveals a relevant mismatch among the values extracted on different samples at negative voltages. This is mainly due to

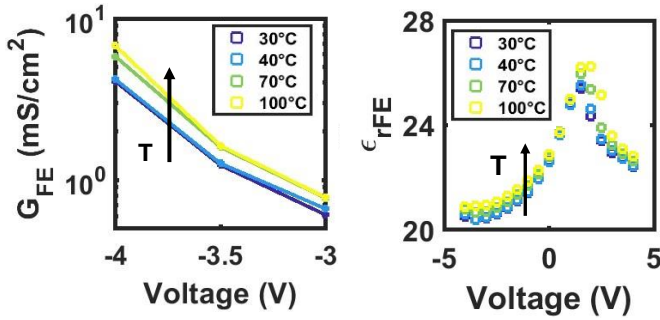


Fig. 11 – Temperature dependence of extracted HZO parameters. The device has $t_{DE} = 1.5 \text{ nm}$, $A = 6.16 \cdot 10^{-4} \text{ cm}^2$. As expected, the permittivity of the ferroelectric increases with the temperature, as well as the HZO leakage measured at strongly negative voltages.

the different device states, as different devices underwent different number of cycles or stresses during the experiments, suggesting that the FE defectivity (and the model in general) can be used as an investigation tool for FTJ degradation analysis [20].

Fig. 10 shows the parameters extracted on FTJs with different DE thickness values. Extracted model parameters evidence no particular trend, not even in C_{it} , although the G_p/ω profiles present peaks at different magnitudes. This underlines even further how the typical strategy to estimate the interface trap density (i.e., proportional to the peak magnitude in the G_p/ω profile) [8,9] can lead to misleading predictions, and that a more refined modeling approach is needed. It is worth mentioning that the C_{it} values extracted here (20-50 $\mu\text{F}/\text{cm}^2$) should not be rigidly interpreted as related to traps located exclusively at the IF interface (that would lead to unrealistically high densities $\approx 1 - 3 \cdot 10^{14} \text{ cm}^{-2}$) but rather as an average local volumetric trap density ($\approx 10^{20} - 10^{21} \text{ cm}^{-3}$), since defects across almost the whole stack can respond in C-f/G-f measurements, as shown by advanced multiscale simulations [21], and also play a role in compensating polarization charge.

Finally, temperature dependent measurements have been carried out, performing C-f/G-f measurements in the range 30°C-100°C. Figures 11-12 show that the model, without introducing any constraint, can correctly reproduce the expected temperature dependence of the trap-assisted leakage in the FE (found to be close to that experimentally measured in HfO_2 RRAMs [22] by extracting the activation energies at negative bias voltages) and of the FE permittivity [23]. In particular, the derived ϵ_{rFE} temperature dependence profile is in qualitative agreement with expectations and with the trends in the literature, while a quantitative agreement with other reports can be achieved considering an A_f consistent with simulations [13, 20].

VII. CONCLUSIONS

We introduced and validated an advanced FTJ small-signal model that accounts for separate leakage contributions in the FE and DE layers, frequency dependence of DE permittivity, voltage dependence of FE permittivity, series impedance given by the presence of an access device (in our case) or possible stray impedances, and non-uniform crystalline FE phase. The model correctly reproduces C-f/G-f measurements up to 10MHz taken on devices with different DE thicknesses and in different conditions. The possibility to isolate and study

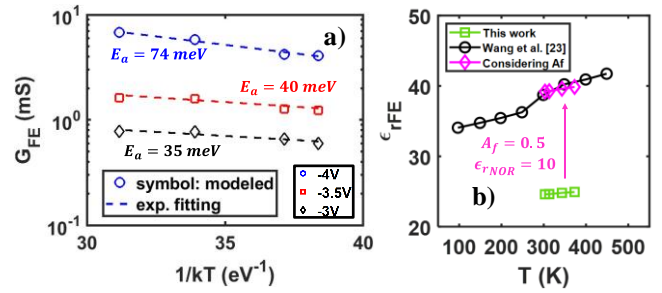


Fig. 12 – a) Arrhenius plot and activation energies derived by FE conductance at strongly negative voltages, (Fig. 10). b) FE permittivity extracted temperature dependence (green), and its projection considering $A_f = 0.5$ (magenta). Data are taken at 0 V bias. For reference, fully orthorhombic data from the literature [23] are also reported (black).

the impact of each model parameter on the frequency response allows a more refined and dependable investigation of the physical mechanisms occurring in the samples and of the effects of the material properties on the entire device.

Results show that the overall leakage through the stack is dominated by FE defectivity, while high frequency response is given by a complex interplay between the series impedance and DE properties, highlighting that the typically adopted estimation methods for interface trap density may be misleading. This is further confirmed by the modeling of devices with different DE thicknesses, presenting different G_p/ω peaks but similar traps parameters.

Modelling results on temperature dependent measurements allowed also to derive FE parameters trends consistent with other literature reports, confirming the robustness and validity of the proposed FTJ small-signal model.

ACKNOWLEDGMENTS

The authors would like to express gratitude to NaMLab for providing the devices. The work is funded by the H2020 BeFerroSynaptic (GA 871737) project.

The content reflects the authors' results, but not necessarily the opinion of the EC.

REFERENCES

- [1] S. Oh, H. Hwang, and I. K. Yoo, "Ferroelectric materials for neuromorphic computing", *APL Materials* 7, 091109 (2019) <https://doi.org/10.1063/1.5108562>
- [2] Ryu, H., Wu, H., Rao, F. et al. "Ferroelectric Tunneling Junctions Based on Aluminum Oxide/Zirconium-Doped Hafnium Oxide for Neuromorphic Computing", *Sci Rep* 9, 20383 (2019). <https://doi.org/10.1038/s41598-019-56816-x>
- [3] Chen, H., Tang, L., Liu, L., Chen, Y., Luo, H., Yuan, X., & Zhang, D. (2020). "Significant improvement of ferroelectricity and reliability in $\text{Hf}_0.5\text{Zr}_0.5\text{O}_2$ films by inserting an ultrathin Al_2O_3 buffer layer". *Applied Surface Science*, 148737, <https://doi.org/10.1016/j.apsusc.2020.148737>
- [4] J. Hwang, Y. Goh and S. Jeon, "Effect of Insertion of Dielectric Layer on the Performance of Hafnia Ferroelectric Devices," in *IEEE Transactions on Electron Devices*, vol. 68, no. 2, pp. 841-845, Feb. 2021, <https://doi.org/10.1109/TED.2020.3043728>
- [5] L. Benatti and F. M. Puglisi, "Understanding the Reliability of Ferroelectric Tunnel Junction Operations using an Advanced Small-Signal Model," 2021 IEEE International Integrated Reliability Workshop (IIRW), 2021, pp. 1-6, <https://doi.org/10.1109/IIRW53245.2021.9635621>
- [6] B. Max, M. Hoffmann, S. Slesazek and T. Mikolajick, "Direct Correlation of Ferroelectric Properties and Memory Characteristics in

- Ferroelectric Tunnel Junctions," in IEEE Journal of the Electron Devices Society, vol. 7, pp. 1175-1181, 2019, <https://doi.org/10.1109/JEDS.2019.2932138>
- [7] Pešić, M., Fengler, F.P.G., Larcher, L., Padovani, A., Schenk, T., Grimley, E.D., Sang, X., LeBeau, J.M., Slesazek, S., Schroeder, U. and Mikolajick, T. (2016), Physical Mechanisms behind the Field-Cycling Behavior of HfO₂-Based Ferroelectric Capacitors. *Adv. Funct. Mater.*, 26: 4601-4612. <https://doi.org/10.1002/adfm.201600590>
- [8] Y. Qu, J. Li, M. Si, X. Lyu and P. D. Ye, "Quantitative Characterization of Interface Traps in Ferroelectric/Dielectric Stack Using Conductance Method," in IEEE Transactions on Electron Devices, vol. 67, no. 12, pp. 5315-5321, Dec. 2020, <https://doi.org/10.1109/TED.2020.3034564>
- [9] J. Li, Y. Qu, M. Si, X. Lyu and P. D. Ye, "Multi-Probe Characterization of Ferroelectric/Dielectric Interface by C-V, P-V and Conductance Methods," 2020 IEEE Symposium on VLSI Technology, 2020, pp. 1-2, <https://doi.org/10.1109/VLSITechnology18217.2020.9265069>
- [10] Lun Xu, Tomonori Nishimura, Shigehisa Shibayama, Takeaki Yajima, Shinji Migita, and Akira Toriumi, "Kinetic pathway of the ferroelectric phase formation in doped HfO₂ films", *Journal of Applied Physics* 122, 124104 (2017) <https://doi.org/10.1063/1.5003918>
- [11] R. Materlik, C. Künneth, and A. Kersch, "The origin of ferroelectricity in Hf_{1-x}Zr_xO₂: A computational investigation and a surface energy model", *Journal of Applied Physics* 117, 134109 (2015) <https://doi.org/10.1063/1.4916707>
- [12] Abdulazhanov, Sukhrob & Le, Quang Huy & Huynh, Dang Khoa & Wang, Defu & Kämpfe, Thomas. (2019). A mmWave Phase Shifter Based on Ferroelectric Hafnium Zirconium Oxide Varactors. <https://doi.org/10.1109/IMWS-AMP.2019.8880144>
- [13] M. -Y. Kao et al., "Variation Caused by Spatial Distribution of Dielectric and Ferroelectric Grains in a Negative Capacitance Field-Effect Transistor," in IEEE Transactions on Electron Devices, vol. 65, no. 10, pp. 4652-4658, Oct. 2018, <https://doi.org/10.1109/TED.2018.2864971>
- [14] B. Lin, G. Choe, J. Hur, A. I. Khan, S. Yu and H. Wang, "Experimental RF Characterization of Ferroelectric Hafnium Zirconium Oxide Material at GHz for Microwave Applications," 2021 Device Research Conference (DRC), 2021, pp. 1-2, <https://doi.org/10.1109/DRC52342.2021.9467202>
- [15] S. J. Kim, J. Mohan, C. D. Young, L. Colombo, J. Kim, "Ferroelectric TiN/Hf_{0.5}Zr_{0.5}O₂/TiN Capacitors with Low-Voltage Operation and High Reliability for Next-Generation FRAM Applications," 2018 IEEE International Memory Workshop (IMW), 2018, pp. 1-4, <https://doi.org/10.1109/IMW.2018.8388832>
- [16] Halit Altuntas, Kemal Kaplan, Electrical conduction mechanisms and dielectric relaxation in Al₂O₃ thin films deposited by thermal atomic layer deposition, *Materials Science in Semiconductor Processing*, Volume 86, 2018, Pages 111-114, ISSN 1369-8001, <https://doi.org/10.1016/j.mssp.2018.06.027>
- [17] B. Max, M. Hoffmann, S. Slesazek and T. Mikolajick, "Ferroelectric Tunnel Junctions based on Ferroelectric-Dielectric Hf_{0.5}Zr_{0.5}O₂/Al₂O₃ Capacitor Stacks," 2018 48th European Solid-State Device Research Conference (ESSDERC), 2018, pp. 142-145, <https://doi.org/10.1109/ESSDERC.2018.8486882>
- [18] Thakur, Y., Zhang, T., Jacob, C., Yang, T., Bernholc, J., Chen, L. Q., Runt, J., & Zhang, Q. M. (2017). Enhancement of the dielectric response in polymer nanocomposites with low dielectric constant fillers. *Nanoscale*, 9(31), <https://doi.org/10.1039/c7nr01932g>
- [19] Kohlstedt, H. & Pertsev, N. & Contreras, J. & Waser, Rainer. (2005). "Theoretical current-voltage characteristics of ferroelectric tunnel junctions", *Physical Review B*. 72. 10.1103/PhysRevB.72.125341 <https://doi.org/10.1103/PhysRevB.72.125341>
- [20] L. Benatti, P. Pavan and F. M. Puglisi, "Combining Experiments and a Novel Small Signal Model to Investigate the Degradation Mechanisms in Ferroelectric Tunnel Junctions," 2022 IEEE International Reliability Physics Symposium (IRPS), 2022, pp. P6-1-P6-5, <https://doi.org/10.1109/IRPS48227.2022.9764602>
- [21] G. Sereni, L. Vandelli, D. Veksler and L. Larcher, "A New Physical Method Based on CV – GV Simulations for the Characterization of the Interfacial and Bulk Defect Density in High- k /III-V MOSFETs," in IEEE Transactions on Electron Devices, vol. 62, no. 3, pp. 705-712, March 2015, <https://doi.org/10.1109/TED.2014.2385959>
- [22] F. M. Puglisi, A. Qafa and P. Pavan, "Temperature Impact on the Reset Operation in HfO₂ RRAM," in IEEE Electron Device Letters, vol. 36, no. 3, pp. 244-246, March 2015, <https://doi.org/10.1109/LED.2015.2397192>
- [23] D. Wang, J. Wang, Q. Li, W. He, M. Guo, A. Zhang, Z. Fan, D. Chen, M. Qin, M. Zeng, "Stable ferroelectric properties of Hf_{0.5}Zr_{0.5}O₂ thin films within a broad working temperature range", 2019, *Jpn. J. Appl. Phys.* <https://doi.org/10.7567/1347-4065/ab3844>